Mapping vegetation height and identifying the northern forest limit across Canada using ICESat-2, Landsat time series and topographic data

H. Travers-Smith [a,*], N.C. Coops [a], C. Mulverhill [a], M.A. Wulder [b], D. Ignace [c], T.C. Lantz [d]

[a] Department of Forest Resource Management, University of British Columbia, Vancouver, BC V6T 1Z4, Canada
[b] Canadian Forest Service, (Pacific Forestry Centre), Natural Resources Canada, Victoria, BC V8Z 1M5, Canada
[c] Department of Forest Conservation Science, University of British Columbia, Vancouver, BC V6T 1Z4, Canada
[d] University of Victoria, School of Environmental Studies, Victoria, BC V8W 2Y2, Canada

ARTICLE INFO

ABSTRACT

The northern forest-tundra ecotone is one of the fastest warming regions of the globe. Models of vegetation change generally predict a northward advance of boreal forests and corresponding retreat of the tundra. Previous satellite remote sensing analyses in this region have focused on mapping vegetation greenness and tree cover derived from optical multi-spectral sensors. Changes in vegetation structure relating to height and biomass are less frequently investigated due to limited availability of lidar data over space and time in comparison with optical platforms. As such, there is an opportunity to combine lidar and optical remote sensing products for continuous mapping of vegetation structure at high-latitudes, with an emphasis on the forest-tundra transition. In this study, we used lidar data from the Ice, Cloud and land Elevation Satellite (ICESat-2) to classify canopy presence/absence, and predict canopy height across 120 million hectares of the Canadian forest-tundra ecotone at 30 m spatial resolution. Spatially continuous predictors derived from the Landsat satellite archive (2012–2021) and the ASTER (Advanced Spaceborne Thermal Emission and Reflection Radiometer) Digital Elevation Model were used to extrapolate 98th percentile canopy height from the ICESat-2 Land and Vegetation Height (ATL08) product using Random Forests models developed in R (version 4.2.2). Model accuracy was assessed using data from the Land, Vegetation and Ice Sensor (LVIS), a large-footprint airborne lidar system. The overall accuracy of the canopy presence classification was 89%, and canopy presence was detected with 88% accuracy. Models of vegetation height showed an overall R^2 of 0.54 and RMSE of 2.09 m. Finally, we used these methods to map the limit of continuous 3 m forest across Canada and compared our model outputs with forest cover from the MODIS and Landsat Vegetation Continuous Fields datasets. This work demonstrates the challenges and potential for mapping horizontal and vertical vegetation structure within sparse, high latitude forests using both lidar and optical remote sensing data.

1. Introduction

Satellite observations show that circumpolar vegetation composition and productivity are changing in response to rapid increases in air temperature (Beck and Goetz, 2011; Berner et al., 2020a; Orndahl et al., 2022). Notably, changes in vegetation productivity differ across the tundra and boreal biomes. While the tundra has shown increases in productivity driven by shrub expansion and growth (Berner et al., 2020b; Myers-Smith et al., 2011; Myers-Smith and Hik, 2018; Seider et al., 2022), the boreal has shown weaker increases, or decreases in productivity associated with fire and drought stress (Bonney et al., 2018; Sulla-Menashe et al., 2018). The transition region between these two

biomes, described as the forest-tundra ecotone (FTE) covers 1.9 million km² of land and is one of the Earth's largest ecological boundaries (Ranson et al., 2011). The FTE represents a decreasing northward gradient of forest cover and density that transitions to shrub and herbaceous vegetation (Callaghan et al., 2002; Payette et al., 2001). Over thousands of years, the distribution of vegetation in the FTE has shifted in response to cooling and warming periods in climate (Sulphur et al., 2016). Ongoing changes in climate could result in northward advance of the forest-tundra boundary, increases in vegetation stature and changes in community composition (Chapin et al., 2005; Pearson et al., 2013). Pearson et al. (2013) predicts increases in above-ground biomass of 15–42% by 2050 driven by growth and range expansion of woody

shrubs and trees. These changes would have significant impacts on global climate by altering above and below-ground carbon storage (Wilmking et al., 2006) and surface albedo (Chapin et al., 2005). Thus, mapping and monitoring vegetation in the FTE is of importance, both regionally and globally.

Optical satellite datasets derived from AVHRR (Advanced Very High Resolution Radiometer), MODIS (Moderate Resolution Imaging Spectroradiometer), and the Landsat series of satellites have been used to map tree cover (Guo et al., 2020; Montesano et al., 2020; Ranson et al., 2011), and vegetation productivity (Arndt et al., 2019; Berner and Goetz, 2021; Guay et al., 2014; Ju and Masek, 2016) across the circumpolar Arctic and sub-Arctic. For example, the MODIS and Landsat Vegetation Continuous Fields (VCF) products have been used to map the areal extent and recent advances in forest cover within the FTE (Guo et al., 2020; Guo and Rees, 2021; Ranson et al., 2011). Trends in the Normalized Difference Vegetation Index (NDVI) and the Enhanced Vegetation Index (EVI) also suggest that spectral greening (increasing productivity) has occurred along the coldest, sparsely forested margins of the boreal (Berner and Goetz, 2021; Sulla-Menashe et al., 2018). However, the relationship between greening and ground-based vegetation processes in the FTE are not always clear due to weak associations between greening indices and forest cover (Brehaut and Danby, 2018; Loranty et al., 2018; Walker et al., 2021). Furthermore, tree cover from VCF is defined as the amount of skylight intercepted by tree canopies >5 m in height (Montesano et al., 2009). However, trees across the FTE may be as short as 2–3 m, and VCF products have been shown to overestimate tree cover in sparsely forested, shrubby landscapes close to the treeline (Ranson et al., 2011; Timoney and Mamet, 2020).

Integrating multiple types of remote sensing and ground-based datasets can provide insights that extend beyond surface spectral characteristics including changes in land cover (Olthof et al., 2009; Wang et al., 2020), plant functional type (Orndahl et al., 2022), vertical vegetation structure (Bolton et al., 2018a; Margolis et al., 2015; Montesano et al., 2016), and disturbance history (Hermosilla et al., 2015). In particular, structural attributes of vegetation relating to height, volume, and biomass are also important in understanding ecosystem dynamics, and can be estimated from Light Detection and Ranging (lidar) platforms (Lefsky et al., 2002). Small footprint lidar data are typically acquired from Airborne Laser Scanning (ALS) systems to measure canopy height, which can be used to model basal area, stem volume, and aboveground biomass over a range of spatial scales(Bolton et al., 2018b; Goodbody et al., 2021; Margolis et al., 2015; Queinnec et al., 2021). These ALS systems have ground footprints between 0.1 m–25 m and high vertical sampling rates. Thieme et al. (2011) demonstrated that ALS data is capable of detecting small trees >1 m in the forest-tundra ecotone with 90% success.

One important exception to small-footprint ALS is the NASA LVIS (Land, Vegetation and Ice Sensor) instrument, which is an ALS system with a large, 17 m footprint (Blair and Hofton, 2020; Feng et al., 2023). Sensors such as LVIS utilize full waveform measurements, and can fly higher and faster than typical airborne platforms (Lim et al., 2003). LVIS data have been used to derive forest stand height (Kellndorfer et al., 2010) and model above ground biomass (Ni-Meister et al., 2010) in temperate-deciduous and mixed-wood forests. As part of the NASA Arctic-Boreal Vulnerability Experiment (ABoVE) program, the LVIS instrument has also collected data across Alaska and northwestern Canada (Blair and Hofton, 2020). These open-access data have been used to validate canopy height measurements from spaceborne lidar platforms operating at high latitudes (Feng et al., 2023). Given a lack of jurisdictional inventory programs, limited distribution of suitable airports, and fuel costs at high latitudes – spaceborne lidar missions provide a means to augment, and extend airborne lidar acquisitions to larger and difficult to access areas (Coops et al., 2021; Margolis et al., 2015).

Spaceborne lidar missions can provide data that is are freely available and analysis ready at global scales. Compared to ALS systems, spaceborne platforms have larger ground footprints (11 m–70 m) and

much lower sampling frequencies (White et al., 2014; Coops et al., 2021). Lidar missions including the Ice, Cloud and land Elevation Satellite missions (ICESat; Neumann et al., 2019) and the Global Ecosystem Dynamics Investigation (GEDI; Dubayah et al., 2020) have been used to map vegetation height (Lefsky, 2010; Liu et al., 2021; Malambo et al., 2023; Simard et al., 2011) and model above-ground biomass (Margolis et al., 2015; Narine et al., 2019; Nelson, 2010; Ni-Meister et al., 2010) across a range of temperate and boreal ecosystems.

ICESat-2 is currently the only spaceborne lidar system operating at latitudes above 51.5°N (Markus et al., 2017). The ATLAS instrument onboard ICESat-2 uses three pairs of beams to sample vegetation and terrain height every 70 cm along the satellite's path (Markus et al., 2017). Photon returns for each pulse are provided in the ATL03 data product (Global Geolocated Photon Data) and are classified as canopy, top of canopy, or ground. The ATL08 Land and Vegetation Height data product aggregates photon returns into 20 m and 100 m segments in the along-track direction, and provides summary statistics per segment (Neuenschwander and Pitts, 2019). As of Version 5, only 98th percentile height is available for the 20 m segments, however other statistics are reported for 100 m segments including height percentiles, mean, maximum and minimum, (Neuenschwander et al., 2021). Neuenschwander et al. (2020) used ALS data to validate the ATL08 Land and Vegetation Height product within 100 m segments and reported RMSE for terrain and vegetation heights of 0.73 m and 0.56 m, respectively across boreal forests in Finland. As a single-photon counting system, canopy height estimates from ICESat-2 are subject to noise and are influenced by beam strength, time of day, snow cover (Neuenschwander et al., 2022) and terrain complexity (Feng et al., 2023; Zhang and Liu, 2023).

Generating spatially continuous estimates of vegetation height and structure are important goals in forest management and ecosystem monitoring (Coops et al., 2021; Goodbody et al., 2021). A large number of discrete lidar plots from ALS or spaceborne platforms can be used to model continuous structural attributes from optical and radar data (Coops et al., 2021; Lefsky, 2010; Malambo et al., 2023; Matasci et al., 2018; Shah et al., 2020; Sothe et al., 2022; Wulder et al., 2012). For example, Matasci et al. (2018) demonstrated use of a time-series of Landsat imagery to predict structural metrics from ALS across Canada's 650 million hectares (Mha) of forest dominated ecozones using K-nearest neighbor imputation. Machine learning algorithms (Malambo et al., 2023; Narine et al., 2019; Sothe et al., 2022; Zhang and Liu, 2023) and deep learning methods (Shah et al., 2020) are also used to predict lidar-based vegetation structure from Landsat data at varying spatial scales. However, methods extending spaceborne lidar metrics have not focused on model calibration or validation at high latitudes, where canopies are generally much shorter and sparser than at lower latitudes (Zhang and Liu, 2023). Current global vegetation height products using spaceborne remote sensing data tend to overpredict canopy height in the forest-tundra and have higher levels of uncertainty due to a lack of training data at high latitudes and optimizing predictions for taller vegetation(Lang et al., 2023; Lefsky, 2010). The ability to make inferences about vegetation changes in the forest-tundra ecotone with existing canopy height products is currently limited. Zhang and Liu (2023) mapped canopy height using ICESat-2 and Sentinel data within Alaska, however there is still potential to map over larger areas and take advantage of the long temporal continuity of the Landsat record.

To capture the variable and fine-scale nature of changes in vegetation structure across the FTE, there is a need for remote sensing products that capture sufficient detail, are spatially continuous, and validated against fine-scale observations (Timoney, 2022; Timoney and Mamet, 2020). In this analysis, we used the ICESat-2 ATL08 Land and Vegetation Height data product (Neuenschwander and Pitts, 2019) to model canopy presence or absence and height across the Canadian forest-tundra ecotone at 30 m spatial resolution using Landsat surface reflectance, and topographic information. These models were validated against an independent source of ALS lidar data from the LVIS instrument and were

used to map vegetation structure within a study area covering 120 Mha. Finally, we demonstrated the use of these models to map the northernmost limit of continuous forest and identify changes in vegetation structure across the ecotone.

2. Methods

2.1. Study area

In this analysis, we focus on approximately 120 million hectares across the Canadian forest-tundra ecotone within Yukon, Northwest Territories and Nunavut. This region traverses the traditional territories of many distinct northern Indigenous peoples including the Gwich'in, Dene, Inuit and Cree (Fig. 1). Climate, soils and vegetation vary widely across the latitudinal forest-tundra ecotone and along an east to west gradient (Timoney et al., 1992). Our study area includes the Taiga Plains, Taiga Shield and the Southern Arctic ecozones. The Taiga Plains and Taiga Shield ecozones are sometimes referred as "the land of little sticks", as short, cool growing seasons and long, cold winters severely limits vegetation growth and productivity (Ecosystem Classification Group, 2008). Across the study region mean annual temperature and total annual precipitation ranges from approximately −11 to −6 °C and 150–400 mm, respectively (Vincent et al., 2020; Wang et al., 2016). The dominant tree species close to the forest limit are white spruce (*Picea glauca*) and black spruce (*Picea mariana*), which exhibit a gradient of taller denser stands in the south that transition to sparse, isolated stands near the treeline. The Southern Arctic is generally treeless, and is characterized by dwarf, low-shrub and graminoid tundra. Permafrost is continuous in the northwestern part of the study area, but both continuous and discontinuous permafrost are present in the central and eastern parts of the study area.

2.2. Overall workflow

The workflow for this research followed three primary steps: 1) deriving spectral and topographic predictor variables from a time-series of Landsat surface reflectance data and a digital elevation model, 2) spatially joining predictor variables to 98th percentile canopy height (h_canopy) from the ICESat-2 ATL08 Land and Vegetation Height Product, and 3) training and validating two Random Forest models to predict canopy presence or absence and canopy height across the study area (Fig. 2). To validate modeled canopy height and presence we used the LVIS Geolocated Surface Elevation and Canopy Height data product (LVISF2), which provides a range of vegetation structural metrics from full-waveform airborne lidar (Blair and Hofton, 2020). Data processing and analysis were conducted in R (version 4.2.2; R Core Team, 2022) using the terra (Hijmans, 2022b), data.table (Dowle and Srinivasan, 2022), dplyr (Wickham et al., 2022), ranger (Wright and Ziegler, 2017), and arrow (Richardson et al., 2022) packages and plots were made using the ggplot2 package (Wickham, 2016).
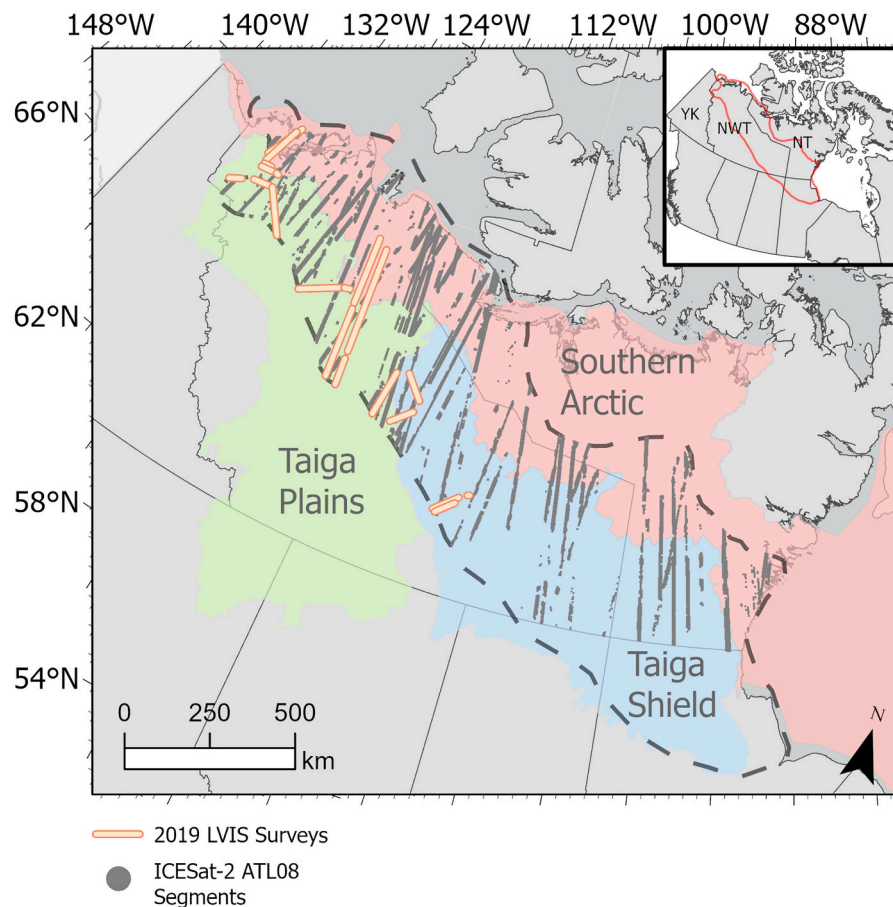

Fig. 1. Map of the northwestern arctic and sub-arctic of Canada. The dashed lines show the extent of the forest-tundra ecotone study area (loosely defined as the region encompassing the Taiga-Southern Arctic boundary). The inset map shows the location of the study area within Canada. The grey points show the 889,366 ICESat-2 ATL08 segments used to train and test the Random Forests models. The orange lines show the extent of the 2019 LVISF2 product used as validation data (Blair and Hofton, 2020).
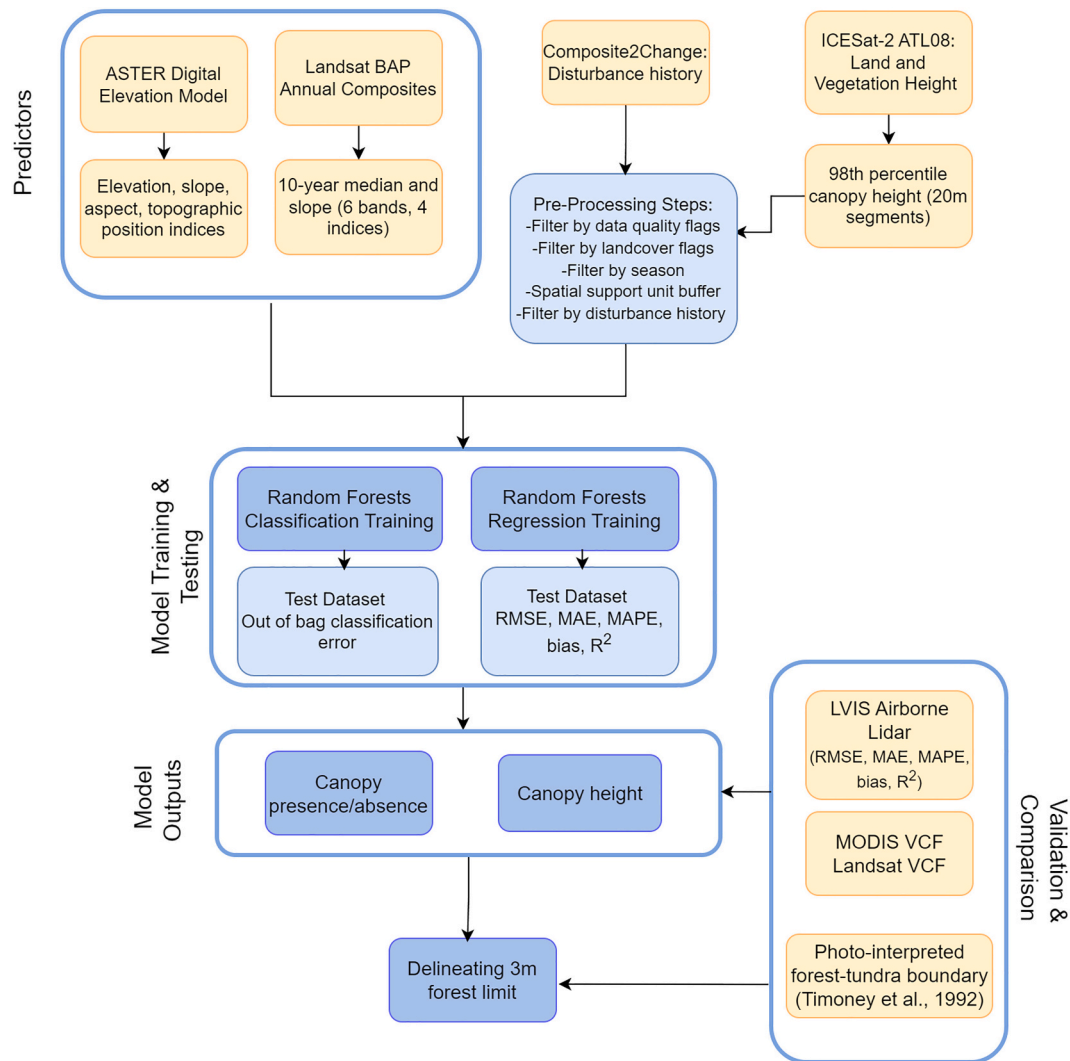
Fig. 2. Flowchart showing methods workflow used to predict and validate canopy presence/absence and canopy height across the forest-tundra ecotone.

2.3. Data

2.3.1. Landsat BAP image composite data

Landsat Best Available Pixel (BAP) composites were generated using data from Landsat-5, 7 and 8 to create annual cloud and gap-free mosaics of surface reflectance across Canada (Hermosilla et al., 2015). BAP composites were created from multiple images acquired over a single growing season, and a pixel scoring function was used to select the best pixel for the season based on sensor, acquisition day, distance to clouds, cloud shadow and atmospheric opacity (White et al., 2014). In this analysis, we defined a 10-year time period from 2012 to 2021 (inclusive), and calculated the median BAP reflectance and the linear slope across six Landsat spectral bands (red, green, blue, NIR, SWIR1, SWIR2), and four indices, Tasseled Cap Brightness (TCB), Tasseled Cap Wetness (TCW), Tasseled Cap Greenness (TCG) and the Enhanced Vegetation Index (EVI). Tasselled Cap transformations were calculated using the equations in Hermosilla et al. (2022) and have been shown to be sensitive to high latitude vegetation change and a range of land cover types (Chen et al., 2021; Fraser et al., 2014). We used a ten-year period to capture temporal trends in spectral reflectance and account for noise along a pixel time series. The combination of two metrics (median and slope) and ten bands/indices yielded a total of 20 variables for modeling canopy presence and height (Table 1). The 2012–2021 period was chosen to correspond with the ICESat-2 data acquired from 2019 to

Table 1
Spectral and topographic predictor variables used to train Random Forests models.

Variable	Time period
Spectral bands (Landsat)	
Blue, green, red, NIR, SWIR1, SWIR2	10-year median, 10-year slope
Spectral Indices (Landsat)	
EVI, TCB, TCW, TCG	10-year median, 10-year slope
Topographic (ASTER)	
Elevation, slope, aspect, roughness, Topographic Position Index (TPI)	–

2021. Prior to modeling, we used the Landsat Composite-2-Change (C2C) data product (Hermosilla et al., 2016) to remove pixels that experienced a stand replacing disturbance between 2012 and 2021.

2.3.2. ICESat-2 ATL08 data

ICESat-2 is a NASA spaceborne lidar platform launched in 2018 to characterize the structure of the Earth's ice caps, vegetation and ground surface (Markus et al., 2017). The ATLAS instrument onboard ICESat-2 uses three pairs of green (532 nm) lasers and a single-photon counting system (Markus et al., 2017). The lasers illuminates the ground every 70

cm along the satellite's path, with each pulse corresponding to a circular footprint approximately 11 m in diameter (Magruder et al., 2021). The outgoing laser is organized into strong and weak beams, with approximately four times more photon returns expected from the strong beams compared to the weak beams (Neuenschwander et al., 2022). Within the boreal forest, the strong beam normally returns between zero and two photons per footprint (Neuenschwander et al., 2022). Geolocated photon returns are then classified as ground, canopy, top of canopy or noise using the DRAGANN algorithm (Neuenschwander and Pitts, 2019). The ATL08 aggregates classified photon returns into 100 m and 20 m segments along the satellite's ground track, and calculates topographic and canopy height metrics within each segment (i.e. mean, median, standard deviation and percentiles; Neuenschwander and Pitts, 2019).

We used the 98th percentile canopy height (h_canopy) within 20 m segments to correspond with the spatial resolution of Landsat pixels (30 m). ATL08 data (Version 5) were downloaded from NASA's National Snow and Ice Data Center (version 5; Neuenschwander et al., 2021). ATL08 segments were filtered based on quality control flags within the data product, (i.e. water, blowing snow, clouds), and the terrain quality flag (terrain_flg), which determines if the estimated ground height deviates beyond an acceptable threshold from a reference DTM. Due to the low number of photon returns expected from sparse vegetation, we only used data acquired by the strong beams (Neuenschwander et al., 2022).

As a single photon counting system operating in the visible wavelength range, solar background noise (i.e. photons scattered by the atmosphere) can significantly impact the ability of the DRAGANN algorithm to separate signal and noise photon returns (Neuenschwander and Pitts, 2019). To improve the signal to noise ratio and resulting canopy height estimates, Neuenschwander et al. (2022) recommend using data acquired at night. Acquisitions from peak growing season (mid-summer) are also preferred in the literature due to greater canopy cover (Mulverhill et al., 2022; Neuenschwander et al., 2022). As much of our study area experiences nearly 24 h of daylight in the summer, we compared ATL08 canopy height retrievals from the summer (July–August) and winter (December–January) against LVISF2 from the same region. Wintertime acquisitions can be collected in darkness, but vegetation canopies are expected to be snow covered. Overall, winter acquisitions showed better agreement with LVIS canopy heights (see section 3.1) and further analysis was conducted with ATL08 segments collected from December 2019 to January 2020. Across the study area we retained a total of 889,366 segments distributed across all ecozones. Overall, 52%, 17.5% and 30.5% of segments were located in the Southern Arctic, Taiga Plain and Taiga Shield ecozones, which correspond to 34%, 14% and 47% of the total study area, respectively.

2.3.3. LVISF2 validation data

The LVIS instrument is a full-waveform lidar system generally flown at an altitude of 10 km (Blair and Hofton, 2020). The laser footprint on the ground varies between 10 m and 25 m and data is collected along 2 km wide transects. The LVIS Level-2 Geolocated Surface Elevation and Canopy Height Product (LVISF2; Version 1) contains geolocated coordinates and canopy metrics calculated from the full-waveform measurements. In this study, we used approximately 33,000 km^2 of LVIS data acquired as part of NASA's Arctic-Boreal Vulnerability Experiment (Fig. 1). Data covering the Canadian forest-tundra ecotone were acquired on four dates in 2019: July 15, July 16, July 25 and August 8. The LVISF2 data product is delivered as points on a 10x10m grid. We extracted maximum canopy height and height at the 95th and 98th percentiles in each grid cell and aggregated the data to match the spatial resolution of Landsat based on the maximum LVIS height percentiles within a 30 m pixel.

2.3.4. ASTER global digital elevation model

Five topographic variables (elevation, slope, aspect, roughness, and Topographic Position Index) were derived from the ASTER Global

Digital Elevation Map at 30 m spatial resolution (Tachikawa et al., 2011; Version 2). Slope, aspect, roughness and Topographic Position Index (TPI) were calculated from the DEM using the adjacent eight pixels in R using the terrain function in the raster package. Roughness is calculated as the difference between the maximum and minimum elevation of a pixel and its neighbours, and TPI is the difference in elevation between a pixel and the mean of its neighbours (Hijmans, 2022a).

2.3.5. Comparison with existing maps

We compared our maps of canopy height and presence to the three independent data sources: the MODIS Terra Vegetation Continuous Fields dataset (DiMicelli et al., 2015), Landsat Vegetation Continuous Fields dataset (Sexton et al., 2013), and fine-scale photo interpretation of the Canadian forest-tundra transition by Timoney et al. (1992). The MODIS VCF dataset represents the sub-pixel fraction of tree cover, non-treed vegetation and non-vegetated surfaces at 250 m resolution generated at an annual time step from 2000 to 2020. The Landsat VCF dataset represents the sub-pixel fraction of forest >5 m in height across the years 2000, 2005, 2010 and 2015. The Timoney et al. (1992) mapping represents the boundaries of the forest-tundra ecotone acorss western and central Canada, interpreted from 1314 air photos. Boundaries for the forest limit, forest-tundra and tree limit were defined using the 1:1000, 1:1 and 1000:1 ratio of forest to tundra land cover, respectively. This work represents the most comprehensive and high-resolution mapping effort of the Canadian FTE using high resolution air photo interpretation.

2.4. Modeling canopy presence and canopy height

We defined a spatial support unit (SSU) around each ATL08 segment centerpoint as a 20 m circular buffer and extracted spectral attributes (10-year median and slope) and topographic information (elevation, slope, roughness, TPI, and aspect) for pixels intersecting with a given SSU. The mean value of each variable within the SSU were joined to the canopy height attributes of each segment. We also used the C2C data product to extract information related to disturbance history for each SSU (Hermosilla et al., 2016). Segments within undisturbed and spectrally homogenous SSUs (defined as <10% coefficient of variation of spectral values) were selected for modeling canopy presence and canopy height. We used homogenous SSUs to ensure that models were trained on a minimum number of pixels representing sudden spatial changes in landcover or mixed land cover types (Mulverhill et al., 2022).

Our modeling approach used two steps 1) a Random Forests classification model to predict canopy presence or absence, and 2) a Random Forests regression model to predict canopy height. Random Forests models were trained using the 20 spectral and 5 topographic variables as predictors in the R package ranger (Wright and Ziegler, 2017). First, we classified ATL08 segments as 'canopy present' or 'canopy absent' based on the number of canopy photon returns and the segment land cover flag (segment_landcover). Segments were classified as canopy absent when there were fewer than four canopy, or top of canopy photon returns in the 20 m segments (i.e. canopy height is assigned 'NA' in the ATL08 product; Neuenschwander et al., 2021), and where the segment land cover was either 'herbaceous', 'moss and lichen' or 'bare sparse vegetation'. This land cover classification is based on the 2019 Copernicus Global Land Cover dataset at 100 m spatial resolution, which has been spatially joined to ATL08 segment meta data. The global producers accuracy for these classes are 71.8%, 42.0% and 91.7%, respectively (Buchhorn et al., 2020). The Random Forests classification model was trained to predict canopy presence and absence using an even sample of SSU's by canopy presence class ($n = 50,000$ per class). Next, we trained a Random Forests regression model to predict canopy height. To ensure the entire range of canopy height was represented in the model, segments were grouped into clusters based on height using the k-means function in R, and an equal number of samples were drawn from each cluster ($n = 30,000$). Pixels where the probability of canopy presence

was <0.5 were assigned a height of 0.

To assess model performance, we extracted the out of bag classification accuracy for the canopy presence model and the coefficient of determination (R^2) and the root mean square error (RMSE) from the canopy height model. Next, the models were tested on a dataset of all undisturbed segments (including segments with heterogenous SSUs). We evaluated model performance using Mean Absolute Error (MAE), Mean Absolute Percent Error (MAPE), Root Mean Square Error (RMSE) and R^2 for the entire dataset and within height classes <2 m (low stature veg), 2-5 m (small trees), 5-10 m (treed), >10 m (tall trees). The canopy presence model was tested on a dataset of 200,000 segments split evenly between the canopy present and absent classes. The canopy height model was tested on 120,000 segments, which were first clustered by height with an equal number of samples drawn from each cluster.

2.5. Model validation using LVISF2

We used the LVISF2 dataset to further evaluate the performance of the Random Forest canopy presence and height models. In total, there were 126 LVISF2 segments across the study area. As the input Landsat surface reflectance layers represents a 10-year median, we removed pixels that underwent a stand-replacing disturbance within the 2012–2021 time period. For undisturbed pixels where a canopy was present, we evaluated canopy height predictions using MAE, RMSE, MAPE and bias against LVIS 98th percentile canopy height, and examined error statistics across different height classes (0-2 m, 2-5 m, 5-10 m and > 10 m). To understand vegetation structure in pixels where the model did not detect a canopy, we calculated summary statistics across the LVIS canopy height metrics for pixels in the canopy absent class.

2.6. Delineating continuous forest

From the resulting canopy height and presence maps, we used an automated workflow to delineate the northernmost boundary of continuous forest >3 m in height (Payette et al., 2001; Timoney et al., 1992). First, we calculated average canopy height within 1 km grid cells

then classified each cell using a 3 m threshold. Next, simplified polygons were created from the classified raster using the Raster to Polygon tool in ArcGIS Pro (version 2.9.5). From these polygons, the Buffer and Generalize Line tools were used to create smoothed continuous boundaries representing 3 m canopy height. This boundary was then compared to mapping of the forest-limit, forest-tundra and tree limit by Timoney et al., (1992; Fig. 6).

3. Results

3.1. Impact of snow cover and daylight on ATL08 data

Overall, median canopy height measured using ICESat-2 were higher (3.92 m) than LVIS (2.15 m). Wintertime ICESat-2 data showed better agreement than data acquired in the summer, with median heights of 3.81 m and 4.02 m, respectively (Fig. 3). Across the study area, LVIS canopy height ranged from 0.57 to 21.87 m, while wintertime and summertime ICESat-2 data ranged from 0.54 to 31.34 m and 0.52–16.32 m. Summer and winter ATL08 retrievals were similar for vegetation within the continuous forest at lower latitudes, but diverged north of 68°N as canopy heights decreased (Fig. 3). Fig. 3 indicates that median LVIS canopy height fell below 3 m in the 67.7-68 N latitudinal bin (Fig. 3). North of 68°N, wintertime ICESat-2 data more closely followed declines in canopy height apparent in the LVIS data (Fig. 3). Median wintertime ICESat-2 data fell below 3 m in the 68–68.3 N range, but summertime data did not decrease to 3 m until the 68.6–68.9 N range (the northernmost latitudinal bin).

3.2. Mapping canopy presence and height

We applied the Random Forests models to map spatial variation in canopy height and presence at 30 m resolution across the Canadian forest-tundra ecotone (Fig. 4). Overall, this map shows the expected transition from high and continuous canopies in the south, to lower and discontinuous canopies in the north (Fig. 4). Within the Taiga Plain, Taiga Shield and Southern Arctic ecoregions, canopy was detected in
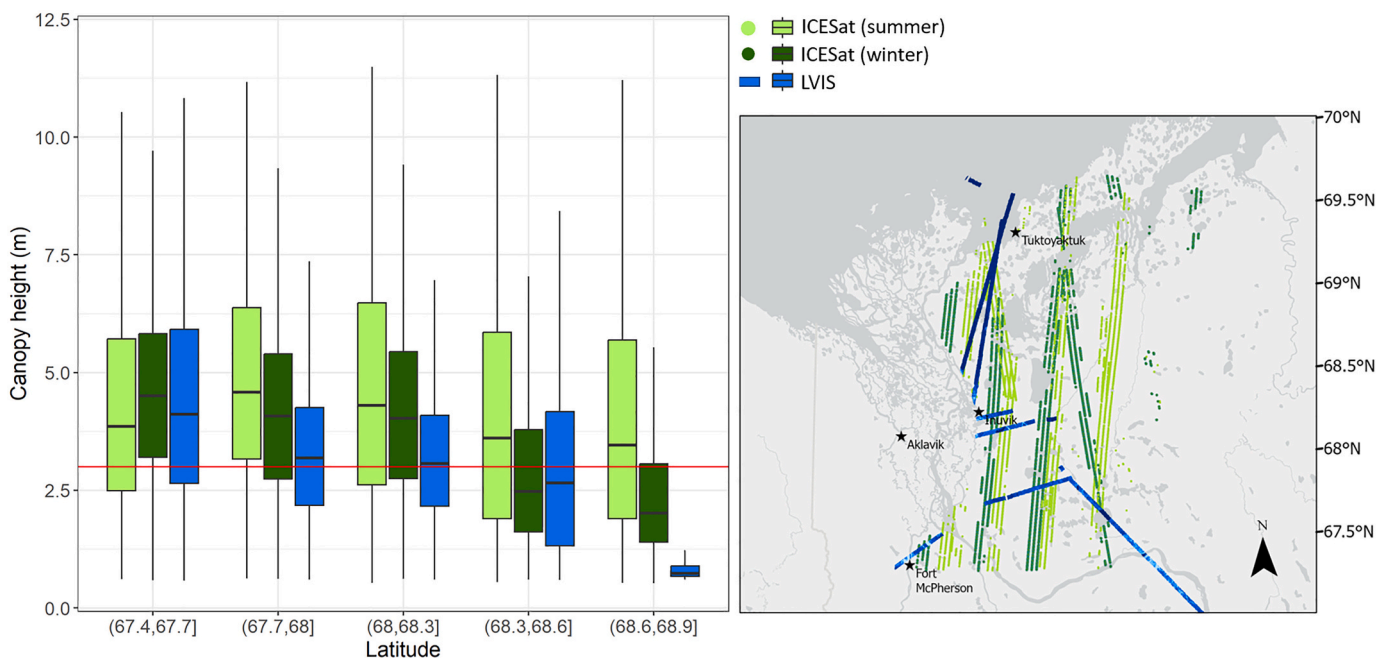

Fig. 3. Boxplots (left) showing height distribution for summer (July–August) and winter (December–January) ICESat-2 ATL08 98th percentile canopy height and LVIS 98th percentile canopy height by increasing latitude. The red line shows the 3 m height limit. The map (right) shows the distribution of ICESat segments (light green and dark green points) and LVIS transects (blue) across the forest-tundra ecotone. (For interpretation of the references to colour in this figure legend, the reader is referred to the web version of this article.)
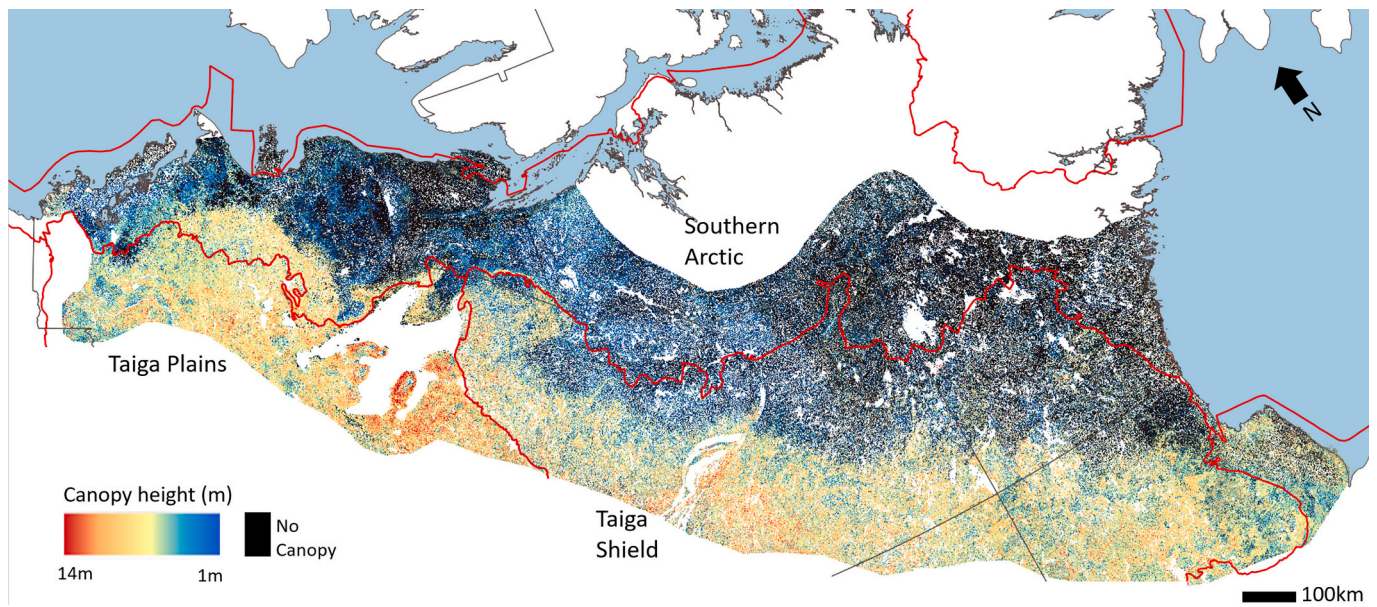
Fig. 4. Map of canopy height and presence across the Canadian forest-tundra transition at 30 m spatial resolution. The red borders show the extent of the Taiga Plain, Southern Arctic and Taiga Shield ecoregions. White areas represent water and areas outside the study region.
(For interpretation of the references to colour in this figure legend, the reader is referred to the web version of this article.)

86%, 58% and 21% of pixels, respectively. The average height for pixels with a canopy was 5.37 m. The distribution of canopy height also varied across ecoregions (Fig. 5). Overall, the Southern Arctic had the lowest canopy heights with a mean of 4.14 m. The Taiga Plain and Taiga Shield showed similar height distributions, with average canopy heights of 5.99 m and 5.47 m, respectively.

Across a 300 km transect crossing the boundary between the Taiga Plain and Southern Arctic, our predictions of the 98th percentile canopy height follow similar declines in tree cover derived from the MODIS and Landsat VCF datasets. The fitted trend in canopy height along the transect can be used to define the width of the transition region between the forest and tundra. For example, canopy height begins to decrease towards 0 m at 155 km along the transect and reaches 0 m at 260 km

Fig. 5. Density plot of the probability density function of canopy height (m) for across the Southern Arctic, Taiga Plains and Taiga Shield ecoregions. Note this only includes pixels where the probability of canopy presence was >0.5.

(Fig. 6). Within this transition (155–260 km), region tree cover ranges from 0 to 12% and 0–10% from MODIS and Landsat VCF, respectively.

The automatic delineation of continuous 3 m forest extent (Fig. 7) corresponds well with the 1:1 forest-tundra boundary mapped by Timoney et al. (1992). Within aggregated 1 km cells, 99% of forested patches are below the 1:1000 tree limit defined by Timoney. Two clusters of forested cells totaling 50 ha in area were mapped above the tree limit. Subsequent examination of these areas on high resolution WorldView-2 imagery from 2019 show that they are likely unforested wetlands.

3.3. Random forests model assessment

Overall, the Random Forests models showed strong predictive accuracy for spectrally homogenous SSUs used for model training. The out of bag error for the Random Forests classification of canopy presence or absence was 7.3%, with 8.7% error in canopy absence class and 5.8% error in canopy presence class. For the canopy height regression model, the R^2 was 0.55 and the RMSE was 1.92 m. Compared with the dataset used to train the models, both models showed slightly reduced performance on a testing dataset containing samples of the remaining SSU's, including SSU's with a high coefficient of variation. Across both classes, the canopy presence/absence model had an 11% misclassification rate, with 12% error in the canopy presence class and 9% in the canopy absence class ($n = 100,000$ per class). The most important variables for predicting canopy presence or absence were median surface reflectance in the SWIR1 band, median TCB and median TCW.

The canopy height model had an overall R^2 of 0.54 and RMSE of 2.09 m ($n = 120,000$; Table 2). Model performance was greatest for canopies between 5 and 10 m, with an RMSE of 1.56 m and MAPE of 17% (Table 2), and approximately 45% of segments across the entire dataset fell within this range (Table 2). The canopy height model generally underpredicted canopies exceeding 10 m in height (bias: −3.48 m, MAPE: 28%; Table 2) and overpredicted heights below 2 m (bias: +1.64 m, MAPE: 137%; Table 2). Across ecozones, the Taiga Plains showed the best performance with MAPE of 34.8% compared with the Taiga Shield and Southern Arctic with MAPE of 55.5% and 61.1%, respectively (Table 2). This likely reflects the higher mean canopy height across the Taiga Plains, resulting in greater overall accuracy. For the canopy height
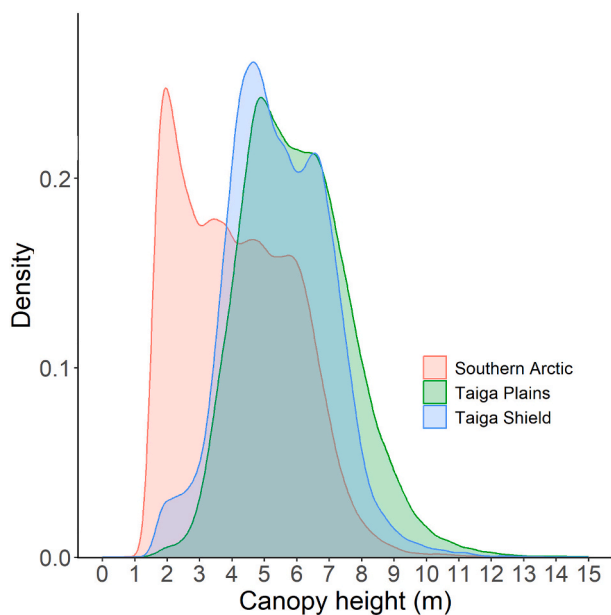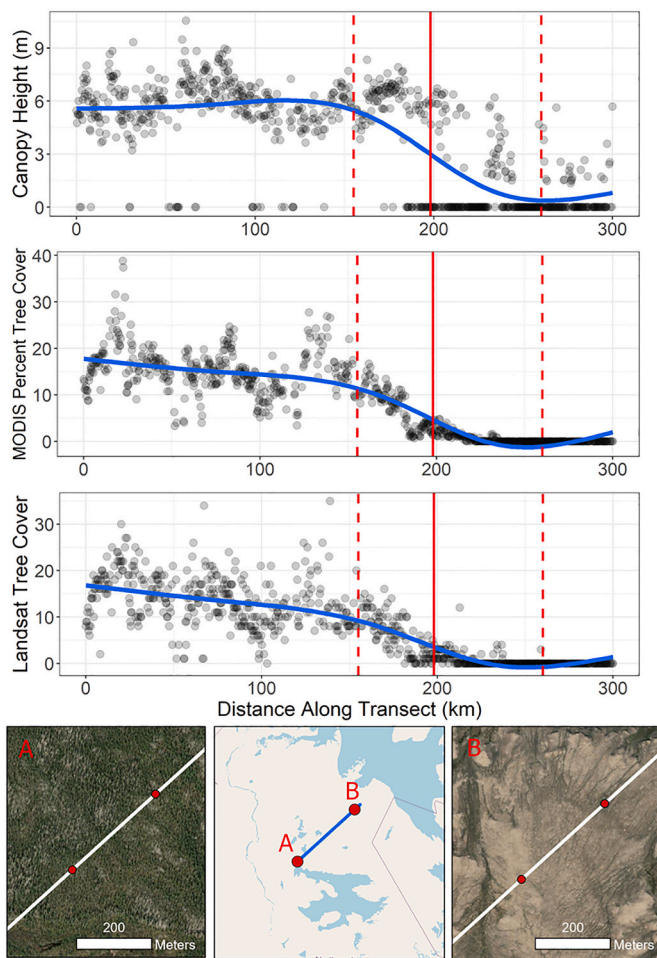
Fig. 6. Modeled 98th percentile canopy height, MODIS VCF Percent Tree Cover and Landsat VCF Tree Cover at 250 m intervals along a transect covering the forest-tundra ecotone (top). The blue line shows the smoothed trend in height and cover fit using a Generalized Additive Model. The dashed red lines show the approximate width of the forest-tundra ecotone and the solid line indicates the limit of continuous 3 m canopy height. The inset maps show high resolution satellite imagery from WorldView-2 imagery for two locations along the transect (bottom). (For interpretation of the references to colour in this figure legend, the reader is referred to the web version of this article.)

regression model, the most important variables were median TCB, and median surface reflectance in the NIR and SWIR2 bands.

3.4. Independent validation using LVIS

Overall, LVISF2 98th percentile height showed moderate agreement with the Random Forests canopy height predictions with an R^2 value of 0.44 and an overall RMSE of 2.69 m (Table 3; Fig. 8). Modeled canopy heights were most accurate in the 5–10 m range, with RMSE of 1.74 m and MAPE of 18.8% (Table 3). Model performance decreased when predicting the highest and lowest canopies, where canopies <2 m were overestimated (Bias: +3.23 m) and canopies >10 m were underestimated (Bias: −3.62 m; Table 3). The distribution of continuous LVIS canopy heights were distinct for pixels classified with and without a canopy present (Fig. 9). The mean and range of canopy height was smaller for the canopy absent class compared to the canopy present class (Fig. 9). For pixels where the Random Forests classification model did not predict a canopy, the mean LVIS 98th percentile height was 1.20 m (Fig. 9).

4. Discussion

Lidar observations play an important role in understanding global changes in vegetation structure (Schimel et al., 2015). In particular, canopy height derived from lidar can be used to quantify above-ground biomass and carbon storage (Lefsky et al., 2002; Simard et al., 2011). However, lidar data acquired by airborne sensors are limited in spatial extent, and data from spaceborne platforms are not spatially continuous. Several approaches have been used to successfully extrapolate lidar observations from ICESat, GEDI, and ALS over broad areas using passive remote sensing products (Coops et al., 2021; Matasci et al., 2018; Wulder et al., 2012). For northern ecosystems, ICESat-2 is the only spaceborne ranging-lidar system operating above 51.5° latitude where small footprint ALS data is limited. In this research, we integrated ICESat-2 canopy height estimates with Landsat BAP composites to produce maps of canopy presence and height across 120 million hectares of the Canadian forest-tundra ecotone at 30 m spatial resolution. We demonstrated the use of these maps to derive the limit of continuous 3 m forest and map variation in vertical structure across the ecotone. As this approach exclusively uses spaceborne remote sensing products, it can be applied to other areas of the circumpolar and can be updated as new data from the Landsat and ICESat-2 missions becomes available.

4.1. Model performance and considerations when using ATL08 data at high latitudes

Error metrics show that our workflow was effective in classifying canopy presence and predicting height. Overall, canopy presence was detected with 88% accuracy and the canopy height model showed a MAE of 2.10 m and R^2 of 0.45 when compared to independent ALS data. These values are consistent with similar work by Malambo et al. (2023) and Sothe et al. (2022) who also modeled ICESat-2 canopy heights using Landsat data in Texas and forested ecoregions of Canada. These studies reported MAE of 2.09 m and 3.4 m, and R^2 of 0.36 and 0.46, respectively. Similarly, Narine et al. (2019) used ICESat-2 to model above-ground biomass using Random Forests and deep learning methods, achieving R^2 values of 0.64–0.67 in a southern pine forest. Recently, Lang et al. (2023) used GEDI, Landsat and Sentinel-2 data to generate spatially continuous estimates of global canopy height. However, these models generally show higher predictive uncertainty in the forest-tundra due to the lack of GEDI training data at high latitudes and model optimization for higher stature vegetation (Lang et al., 2023). Canopy height estimates were validated using LVIS data for three tiles within northern Canada, and Lang et al. (2023) reported RMSE of 2.8 m, 4.6 m and 5.3 m for tiles with average heights of 4.3 m, 8.5 m and 7 m, respectively. For canopies between 2 and 5 m our models show similar RMSE (2.36 m), but show more substantial improvements for canopies in the 5-10 m range with RMSE of 1.74 m and bias of −0.33 m. Our model outputs are developed on localized training samples and are also not impacted by tiling effects reported by Lang et al. (2023) at high latitudes, thus making them more appropriate for continuous mapping of the forest limit.

Our method differs from previous analyses by modeling canopy presence or absence, and then estimating height where a canopy was present. This step is important in the forest-tundra ecotone where the distribution of vegetation is patchy and exhibits a strong gradient across the ecotone (Timoney et al., 1992). Our approach also allows canopy presence to change over time, as it does not rely on ancillary data or static maps of forest cover. For pixels in the canopy absent class, the mean LVIS height at the 98th percentile was 1.20 m, suggesting that the classification was ecologically meaningful as these pixels likely represent low-stature shrub and herbaceous vegetation.

While combining height and presence maps allows us to mask regions without a detectable canopy, misclassification in the canopy presence layer can result in overestimation of vegetation height at some tundra sites above the tree limit. Land cover with different vegetation
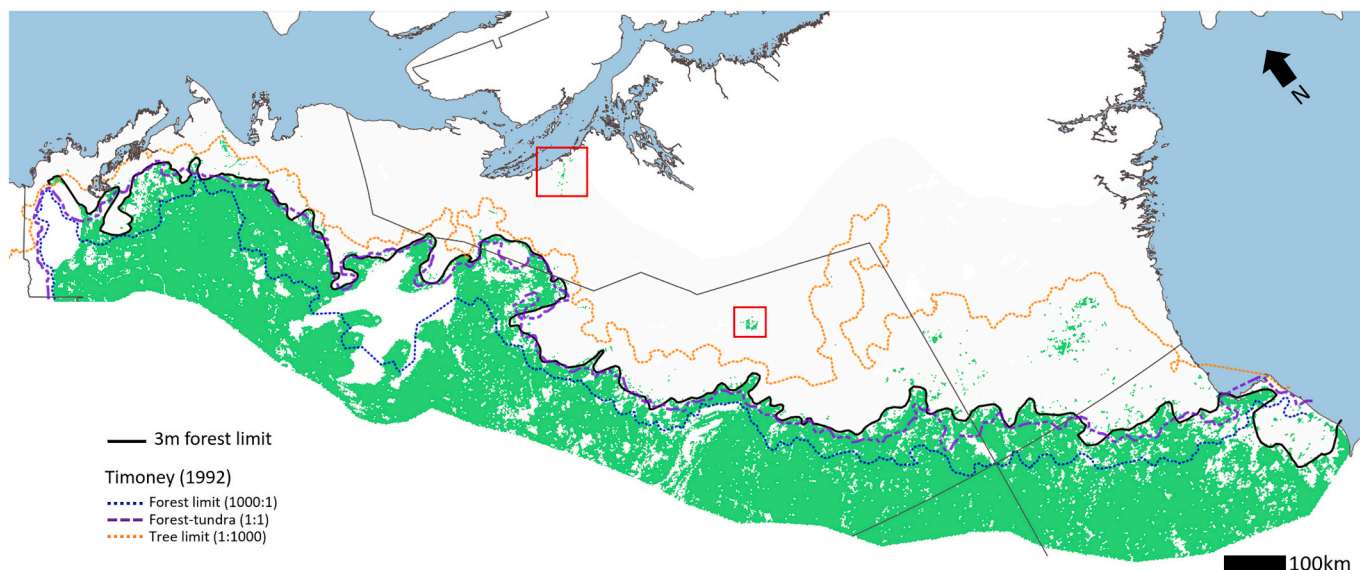
Fig. 7. Map of 3 m canopy distribution, green colour indicates average height of at least 3 m in a 1 km grid cell. The black line delineates the northern extent of continuous forest (the southern extent of continuous forest extends beyond the study area). The dashed lines show the forest limit, forest-tundra and tree limits mapped by Timoney et al. (1992). Red boxes show non-spatially congruous regions above the tree limit that were examined using high-resolution (<1 m spatial resolution) WorldView-2 imagery. (For interpretation of the references to colour in this figure legend, the reader is referred to the web version of this article.)

Table 2

Mean Absolute Error (MAE), Mean Absolute Percent Error (MAPE), Root Mean Square Error (RMSE), and bias for the Random Forests regression model predicting canopy height on a testing dataset containing all undisturbed ATL08 segments with a canopy present. Error metrics are stratified by height and ecozone. The overall r^2 was 0.54 (n = 120,000).

Height Class	MAE (m)	MAPE (%)	RMSE (m)	Bias (m)	Proportion of all ATL08 segments
<2 m	1.64	137	2.28	+1.62	17%
2-5 m	1.51	48.9	1.94	+1.26	34%
5-10 m	1.20	16.9	1.56	+0.60	45%
>10 m	3.5	28.1	4.74	−3.48	4%
Ecozone					
Southern Arctic	1.35	61.1	2.00	0.43	52%
Taiga Plains	1.43	34.8	1.89	0.19	17%
Taiga Shield	1.57	55.5	2.16	0.56	27%
Overall	1.50	60.53	2.09	0.40	–

Table 3

Mean Absolute Error (MAE), Mean Absolute Percent Error (MAPE), Root Mean Square Error (RMSE) and bias of canopy height predictions and LVIS 98th percentile canopy height. The overall R^2 was 0.45 (n = 30,000).

	MAE (m)	MAPE (%)	RMSE (m)	Bias (m)	Proportion of all LVIS 30 m pixels
<2 m	3.12	288.0	3.67	+3.12	19%
2-5 m	1.98	61.7	2.36	+1.89	41%
5-10 m	1.37	18.8	1.74	−0.33	34%
>10 m	3.66	29.1	4.22	−3.62	4%
Overall	2.10	73.94	2.66	+0.5	–

Fig. 8. Canopy height predicted by Random Forests against the validation dataset, LVIS 98th percentile canopy height. The dashed red line is the 1:1 ratio between observed and predicted values. The colour indicates the number of cases in each hexagon cell. (For interpretation of the references to colour in this figure legend, the reader is referred to the web version of this article.)

structure can appear spectrally similar, contributing to false positives in the canopy presence layer. While 99% of forested grid cells occurred below the 1:1000 tree limit, we observed two small patches of 3 m 'forested' vegetation well above the limit (Fig. 6). Subsequent validation using WorldView-2 imagery from 2019 show that these areas are low-lying wetlands, likely covered by graminoid tundra (<0.2 m in height). These areas both represent wet, vegetated land cover types with
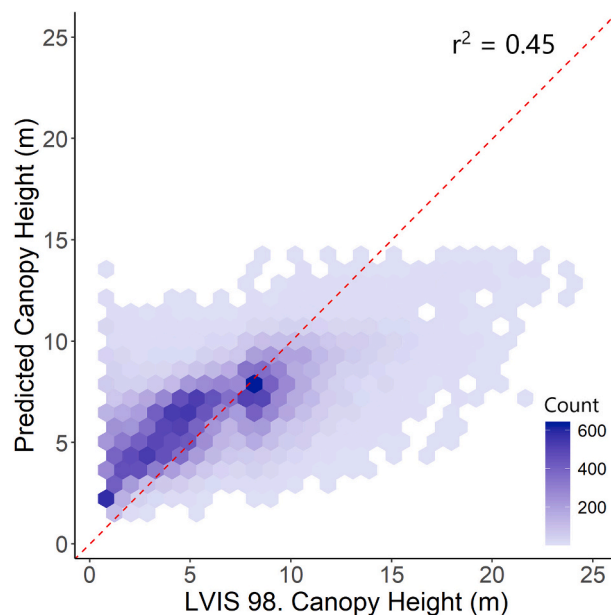
moderate green and NIR reflectance, and thus are spectrally similar to forested wetlands at lower latitudes. This shows the potential for overestimating canopy heights in some green and wetland areas, highlighting the importance of using existing knowledge of forest distribution and high-resolution imagery to confirm anomalous results from remote sensing models. Additional environmental data, such as vegetation phenology (Bolton et al., 2020) or higher spatial resolution land cover maps (Hermosilla et al., 2022) may help separate evergreen and broadleaf shrubs, thus constraining canopy height in these areas.

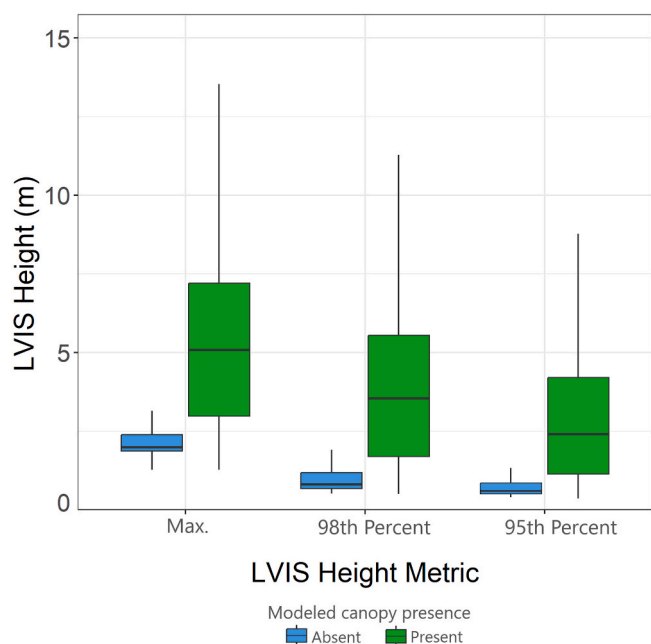The level of agreement between modeled and actual canopy height

Fig. 9. LVIS height metrics (maximum, 98th percentile and 95th percentile height) for pixels classified with (green) and without a canopy present (blue) by the Random Forests model. (For interpretation of the references to colour in this figure legend, the reader is referred to the web version of this article.)

was likely impacted by the modeling algorithm, as well as inaccuracies at the sensor and data level. We observed the most accurate height predictions towards the centre of the height distribution (5-10 m), and decreasing accuracy for very high (>10 m) and low (<2 m) canopies. This is likely due to the Random Forests algorithm, as well as potential inaccuracies at the ATLAS instrument and ATL08 data product levels. First, Random Forests regression models generate predictions using the average output of many decision trees, which tends to pull extreme predictions towards the mean, and truncates the range of predicted values compared to the input dataset (Wright and Ziegler, 2017). This would lead to decreased ability to predict canopy height at the extreme ends of the height distribution. At the sensor and data level, previous studies have also observed underestimation of high canopies and overestimation of low canopies for ICESat-2 canopy height products (Feng et al., 2023; Liu et al., 2021; Neuenschwander and Pitts, 2019). Underestimation of tall canopies likely reflects the point density of the ATLAS sensor (0–2 photon returns per ~11 m footprint), which makes it less likely that photon returns will come from the top of the canopy where foliage is sparse (Neuenschwander et al., 2022; Neuenschwander and Pitts, 2019). The apparent overestimation of shorter canopies is less clear, but may be related to errors associated with estimating terrain height (Feng et al., 2023; Neuenschwander and Pitts, 2019). While ICESat-2 shows improved ability to resolve complex topography compared to the previous ICESat mission, both terrain and canopy heights are likely impacted by steep slopes >30 degrees (Feng et al., 2023; Liu et al., 2021). Due to high relative error for canopies <2 m, our results show limited use of ATL08 data to reliably detect the northern transition of shrub to graminoid tundra present in the northernmost range of our study area.

Due to persistent snow cover, seasonal variation in daylight, and lower overall canopy height, the boreal-tundra vegetation transition poses unique challenges for ICESat-2 canopy height retrievals. In these conditions, we found that season (summer vs winter) substantially impacted ATL08 canopy height estimates, especially for canopies close to the forest limit (Fig. 2). Compared to summertime data, the distribution of canopy height from data collected in the winter showed better agreement with LVIS vegetation heights from the same region (Fig. 2).

These observations likely reflect improved detection of photon returns from the ground and canopy as a result of nighttime acquisitions and greater reflectivity of snow-covered surfaces (Feng et al., 2023; Neuenschwander et al., 2022).

As a single-photon counting system operating with 532 nm (green) lasers, the ATLAS instrument is expected to be susceptible to solar background noise. Nighttime data significantly reduces the number of photon returns scattered in the atmosphere and increases the photon signal to noise ratio (Neuenschwander et al., 2022). Snow cover may also improve canopy height estimates, as greater reflectivity of snow covered surfaces also increases the number of signal returned to the sensor (Neuenschwander et al., 2022). While a higher number of photon returns do not guarantee more accurate canopy height estimates, more signal photons from the ground and canopy should improve the ability of the DRAGANN algorithm to accurately classify photons as ground, canopy and noise (Feng et al., 2023; Neuenschwander et al., 2022). Future work using ATL08 data in circumpolar regions should carefully consider how snow and solar background noise impact the consistency of canopy height estimates.

4.2. Integration with existing knowledge and potential for future work

This work provides a method to improve broad-scale estimates of canopy height and presence at high latitudes. This information could be used to estimate aboveground carbon pools, monitor changes in vegetation structure, or assess wildlife habitat availability (Kurz et al., 2013; Payette et al., 2001). At lower latitudes, canopy height is an important forest structural attribute used to assess aboveground biomass and forest carbon stocks (Kurz et al., 2013; Lefsky, 2010; Lefsky et al., 2002). In Canada, stand level forest inventories are routinely collected across managed portions of temperate and southern boreal regions, but northern boreal forests have more limited and spatially focused monitoring programs (Kurz et al., 2013). Satellite remote sensing products, such as the one presented here, provide a means to estimate canopy height in areas that would be difficult to access otherwise.

This work expands on research using optical remote sensing to monitor vegetation greenness and forest cover in northern ecosystems (Berner et al., 2020b; Olthof et al., 2009; Ranson et al., 2011; Wang and Friedl, 2019), and improves existing models of global canopy height (Lang et al., 2023; Lefsky, 2010; Simard et al., 2011) within the forest-tundra ecotone. Previous work using MODIS Vegetation Continuous Fields indicate that forest cover has increased in some parts of the circumpolar (Guo and Rees, 2021; Olthof and Pouliot, 2010). However more work is needed to validate and train these products at high latitudes, which may overestimate forest cover and height in lightly forested regions with shrubby understories (Ranson et al., 2011; Timoney and Mamet, 2020).

The broad extent (120 mHa) and moderate spatial resolution (30 m) of our maps provide insight into the northern extent of boreal forests, which can be compared to the theoretical limit of forest growth determined by growing season temperature. At a global scale, the extent of continuous forests generally corresponds to growing season air temperatures of 6–7 °C (Körner and Paulsen, 2004). However, despite rapid increases in air temperature over the past century, many latitudinal treelines have not advanced northward with temperature isotherms (Lantz et al., 2019; Maher et al., 2021; Rees et al., 2020; Timoney and Mamet, 2020; Travers-Smith and Lantz, 2020). The difference between temperature isotherms and the current position of the tree or forest line provides an important metric for calibrating models of vegetation change (Mengtian et al., 2017). We used standard geospatial tools to automatically delineate the northernmost boundary of continuous forests across 6000 km. This limit showed strong correspondence with the 1:1 limit forest-tundra boundary previously mapped by Timoney et al., (1992; Fig. 7). Agreement was particularly strong across the western and central parts of the study region and greater differences occurred across the southeastern part of the study area, where our analysis suggests that

the forest-tundra boundary is further north than shown in Timoney et al. (1992). This could be explained by differences in mapping methodology, or by modest increases in forest cover since 1992, the latter of which is supported by analysis of air photos by Timoney and Mamet (2020) in this region.

At a spatial resolution of 30 m, our method will not be sensitive to all nuances in changing vegetation structure across the forest-tundra ecotone. For example, modeled canopy height may not reflect differences in canopy cover and stand density within a 30 m pixel. It is also likely that sparse stands of smaller trees (close to 3 m) are present in pixels where a canopy was not detected. Thus, fine-scale analyses are still required to understand mechanisms of treeline change and spatial patterns identified in coarser resolution satellite images. Increasingly, very high-resolution imagery at the sub-meter scale is becoming available which would be able to support analyses at the level of individual trees and stands (Lantz et al., 2019; Travers-Smith and Lantz, 2020). This kind of fine-scale validation is also important because both increases in tree height and stand density are likely occurring simultaneously across the ecotone, which may or may not result in changes in the northern forest limit (Danby and Hik, 2009; Lantz et al., 2019; Travers-Smith and Lantz, 2020).

Future research using our workflow could also utilize the entire Landsat satellite archive (1984-present) to identify changes in canopy height and presence over multiple decades. Previous research using medium scale satellite data indicate multiple types of ongoing vegetation and land cover transitions at high latitudes. For example, Berner and Goetz (2021) used a time-series of Landsat imagery across the circumpolar and found that significant increases in the NDVI were 1.5–3 times more frequent than decreases in NDVI, especially in regions with colder and less dense tree cover. In Alaska and northwestern Canada, Wang et al. (2020) observed widespread decreases in boreal evergreen forests driven by stand-replacing disturbances, and simultaneous increases in herbaceous and shrub cover in the tundra. By integrating active forms of remote sensing with time-series data, our work has the potential to quantify changes in the structure of northern vegetation, relating to biomass and carbon storage. In particular, estimating terrestrial carbon pools at high latitudes is challenged by sparse sampling networks and high spatial variability (Kurz et al., 2013; Virkkala et al., 2021). Remote sensing tools can be used to generate broad-scale estimates of aboveground carbon storage, which are needed to inform carbon accounting at the national scale (Kurz et al., 2013).

5. Conclusion

In this study, we derived detailed and spatially continuous maps of vegetation structure across 120 mHa of the Canadian forest-tundra ecotone and used these maps to automatically delineate the northern forest limit. We validated predictions of canopy presence and height using fine-scale ALS data and found that our workflow was highly effective in identifying vegetation canopies in the 5–10 m range, representative of short, growth-limited spruce forests in this region. Our findings also highlight limitations and considerations when using ICESat-2 ATL08 Land and Vegetation Height product at high latitudes. As our method relies on freely available satellite remote sensing data it is cost effective, quantitative, repeatable and scalable over large areas. These results can inform large-scale monitoring of climate driven changes in vegetation structure and carbon storage across the circumpolar forest-tundra ecotone.

CRediT authorship contribution statement

H. Travers-Smith: Conceptualization, Formal analysis, Investigation, Methodology, Visualization, Writing – original draft. **N.C. Coops:** Conceptualization, Funding acquisition, Supervision, Writing – review & editing. **C. Mulverhill:** Methodology, Writing – review & editing. **M. A. Wulder:** Supervision, Writing – review & editing. **D. Ignace:** Supervision, Writing – review & editing. **T.C. Lantz:** Supervision, Writing – review & editing.

Declaration of competing interest

The authors declare the following financial interests/personal relationships which may be considered as potential competing interests:

Hana Travers-Smith reports financial support was provided by Natural Sciences and Engineering Research Council of Canada. Nicholas Coops reports financial support was provided by Natural Sciences and Engineering Research Council of Canada. Nicholas Coops reports financial support was provided by Canadian Space Agency.

Data availability

Publicly available datasets used in this study include: ICESat-2 ATL08 version 5 (https://nsidc.org/data/atl08/versions/5), ASTER Global Digital Elevation Model (https://lpdaac.usgs. gov/products/ast14demv003/), LVIS Classic L2 Geolocated Surface Elevation and Canopy Height Product, Version 1 (https://nsidc. org/data/lvisc2/versions/1). Landsat Best Available Pixel (BAP) Composites were generated from Landsat TM and ETM Level-1 Terrain-Corrected Surface Reflectance data (https://earthexplorer.usgs.gov/) and BAP composites used in this analysis are available on request from the authors. R code and datasets supporting this work are also available on Github (https://github.com/hztraver/TreelineMapping). Additional code, data and model outputs are available upon request from the authors.

References

Arndt, K.A., Santos, M.J., Ustin, S., Davidson, S.J., Stow, D., Oechel, W.C., Tran, T.T.P., Graybill, B., Zona, D., 2019. Arctic greening associated with lengthening growing seasons in northern Alaska. Environ. Res. Lett. 14 (12), 125018 https://doi.org/10.1088/1748-9326/ab5e26.

Beck, P.S.A., Goetz, S.J., 2011. Satellite observations of high northern latitude vegetation productivity changes between 1982 and 2008: ecological variability and regional differences. Environ. Res. Lett. 6 (4), 045501 https://doi.org/10.1088/1748-9326/6/4/045501.

Berner, L.T., Goetz, S.J., 2021. Satellite observations document trends consistent with a boreal forest biome shift. Glob. Chang. Biol. https://doi.org/10.1111/gcb.16121 n/a (n/a).

Berner, L.T., Massey, R., Jantz, P., Forbes, B.C., Macias-Fauria, M., Myers-Smith, I., Kumpula, T., Gauthier, G., Andreu-Hayles, L., Gaglioti, B.V., Burns, P., Zetterberg, P., D'Arrigo, R., Goetz, S.J., 2020a. Summer warming explains widespread but not uniform greening in the Arctic tundra biome. *Nature*. Communications 11 (1). https://doi.org/10.1038/s41467-020-18479-5. Article 1.

Berner, L.T., Massey, R., Jantz, P., Forbes, B.C., Macias-Fauria, M., Myers-Smith, I., Kumpula, T., Gauthier, G., Andreu-Hayles, L., Gaglioti, B.V., Burns, P., Zetterberg, P., D'Arrigo, R., Goetz, S.J., 2020b. Summer warming explains widespread but not uniform greening in the Arctic tundra biome. *Nature*. Communications 11 (1). https://doi.org/10.1038/s41467-020-18479-5. Article 1.

Blair, J.B., Hofton, M., 2020. LVIS Facility L2 Geolocated Surface Elevation and Canopy Height Product, Version 1. NASA National Snow and Ice Data Center Distributed Active Archive Center. https://doi.org/10.5067/VP7J20HJQISD.

Bolton, D.K., Coops, N.C., Hermosilla, T., Wulder, M.A., White, J.C., 2018a. Evidence of vegetation greening at alpine treeline ecotones: three decades of Landsat spectral trends informed by lidar-derived vertical structure. Environ. Res. Lett. 13 (8), 084022 https://doi.org/10.1088/1748-9326/aad5d2.

Bolton, D.K., White, J.C., Wulder, M.A., Coops, N.C., Hermosilla, T., Yuan, X., 2018b. Updating stand-level forest inventories using airborne laser scanning and Landsat time series data. Int. J. Appl. Earth Obs. Geoinf. 66, 174–183. https://doi.org/10.1016/j.jag.2017.11.016.

Bolton, D.K., Tompalski, P., Coops, N.C., White, J.C., Wulder, M.A., Hermosilla, T., Queinnec, M., Luther, J.E., van Lier, O.R., Fournier, R.A., Woods, M., Treitz, P.M., van Ewijk, K.Y., Graham, G., Quist, L., 2020. Optimizing Landsat time series length

for regional mapping of lidar-derived forest structure. Remote Sens. Environ. 239, 111645 https://doi.org/10.1016/j.rse.2020.111645.

Bonney, M.T., Danby, R.K., Treitz, P.M., 2018. Landscape variability of vegetation change across the forest to tundra transition of Central Canada. Remote Sens. Environ. 217, 18–29. https://doi.org/10.1016/j.rse.2018.08.002.

Brehaut, L., Danby, R.K., 2018. Inconsistent relationships between annual tree ring-widths and satellite-measured NDVI in a mountainous subarctic environment. Ecol. Indic. 91, 698–711. https://doi.org/10.1016/j.ecolind.2018.04.052.

Buchhorn, M., Lesiv, M., Tsendbazar, N.-E., Herold, M., Bertels, L., Smets, B., 2020. Copernicus global land cover layers—collection 2. Remote Sens. 12 (6) https://doi.org/10.3390/rs12061044. Article 6.

Callaghan, T., Crawford, R., Eronen, M., Hofgaard, A., Payette, S., Rees, G., Skre, O., Sveinbjörnsson, B., Vlassova, T., Werkman, B., 2002. The dynamics of the tundra-taiga boundary: An overview and suggested coordinated and integrated approach to research. Ambio, Spec No 12, 3–5.

Chapin, F.S., Sturm, M., Serreze, M.C., McFadden, J.P., al., et., 2005. Role of land-surface changes in Arctic summer warming. Science 310 (5748), 657–660.

Chen, A., Lantz, T.C., Hermosilla, T., Wulder, M.A., 2021. Biophysical controls of increased tundra productivity in the western Canadian Arctic. Remote Sens. Environ. 258, 112358 https://doi.org/10.1016/j.rse.2021.112358.

Coops, N.C., Tompalski, P., Goodbody, T.R.H., Queinnec, M., Luther, J.E., Bolton, D.K., White, J.C., Wulder, M.A., van Lier, O.R., Hermosilla, T., 2021. Modelling lidar-derived estimates of forest attributes over space and time: a review of approaches and future trends. Remote Sens. Environ. 260, 112477 https://doi.org/10.1016/j.rse.2021.112477.

Danby, R.K., Hik, D.S., 2009. Evidence of recent Treeline dynamics in Southwest Yukon from aerial photographs. ARCTIC 60 (4), 411–420. https://doi.org/10.14430/arctic198.

DiMicelli, C., Carroll, M., Sohlberg, R., Kim, D., Kelly, M., Townsend, J., 2015. MOD44B MODIS/Terra Vegetation Continuous Fields Yearly L3 Global 250m SIN Grid V006 [dataset]. NASA EOSDIS Land Processes Distributed Active Archive Center. https://doi.org/10.5067/MODIS/MOD44B.006.

Dowle, M., Srinivasan, A., 2022. data.table: Extension of 'data.frame'. https://CRAN.R-project.org/package=data.table.

Dubayah, R., Blair, J.B., Goetz, S., Fatoyinbo, L., Hansen, M., Healey, S., Hofton, M., Hurtt, G., Kellner, J., Luthcke, S., Armston, J., Tang, H., Duncanson, L., Hancock, S., Jantz, P., Marselis, S., Patterson, P.L., Qi, W., Silva, C., 2020. The global ecosystem dynamics investigation: high-resolution laser ranging of the Earth's forests and topography. Sci. Remote Sens. 1, 100002 https://doi.org/10.1016/j.srs.2020.100002.

Ecosystem Classification Group, 2008. Ecological Regions of the Northwest Territories – Taiga Shield. (p. viii + 146 pp. + insert map). Department of Environment and Natural Resources, Government of the Northwest Territories. https://www.enr.gov.nt.ca/sites/enr/files/resources/taiga_shield_ecological_land_classification_report_0.pdf.

Feng, T., Duncanson, L., Montesano, P., Hancock, S., Minor, D., Guenther, E., Neuenschwander, A., 2023. A systematic evaluation of multi-resolution ICESat-2 ATL08 terrain and canopy heights in boreal forests. Remote Sens. Environ. 291, 113570 https://doi.org/10.1016/j.rse.2023.113570.

Fraser, R.H., Olthof, I., Kokelj, S.V., Lantz, T.C., Lacelle, D., Brooker, A., Wolfe, S., Schwarz, S., 2014. Detecting landscape changes in high latitude environments using Landsat trend analysis: 1. Visualiz. Remote Sens. 6 (11) https://doi.org/10.3390/rs61111533. Article 11.

Goodbody, T.R.H., Coops, N.C., Luther, J.E., Tompalski, P., Mulverhill, C., Frizzle, C., Fournier, R., Furze, S., Herniman, S., 2021. Airborne laser scanning for quantifying criteria and indicators of sustainable forest management in Canada. Can. J. For. Res. 51 (7), 972–985. https://doi.org/10.1139/cjfr-2020-0424.

Guay, K.C., Beck, P.S.A., Berner, L.T., Goetz, S.J., Baccini, A., Buermann, W., 2014. Vegetation productivity patterns at high northern latitudes: a multi-sensor satellite data assessment. Glob. Chang. Biol. 20 (10), 3147–3158. https://doi.org/10.1111/gcb.12647.

Guo, W., Rees, G., 2021. Correlation between the dynamics and spatial configuration of the circumarctic latitudinal forest-tundra ecotone. Int. J. Remote Sens. 42 (4), 1250–1274. https://doi.org/10.1080/01431161.2020.1826062.

Guo, W., Rees, G., Hofgaard, A., 2020. Delineation of the forest-tundra ecotone using texture-based classification of satellite imagery. Int. J. Remote Sens. 41 (16), 6384–6408. https://doi.org/10.1080/01431161.2020.1734254.

Hermosilla, T., Wulder, M.A., White, J.C., Coops, N.C., Hobart, G.W., 2015. An integrated Landsat time series protocol for change detection and generation of annual gap-free surface reflectance composites. Remote Sens. Environ. 158, 220–234. https://doi.org/10.1016/j.rse.2014.11.005.

Hermosilla, T., Wulder, M.A., White, J.C., Coops, N.C., Hobart, G.W., Campbell, L.B., 2016. Mass data processing of time series Landsat imagery: pixels to data products for forest monitoring. Intern. J. Digital Earth 9 (11), 1035–1054. https://doi.org/10.1080/17538947.2016.1187673.

Hermosilla, T., Wulder, M.A., White, J.C., Coops, N.C., 2022. Land cover classification in an era of big and open data: optimizing localized implementation and training data selection to improve mapping outcomes. Remote Sens. Environ. 268, 112780 https://doi.org/10.1016/j.rse.2021.112780.

Hijmans, R.J., 2022a. raster: Geographic Data Analysis and Modeling. https://CRAN.R-project.org/package=raster.

Hijmans, R.J., 2022b. terra: Spatial Data Analysis. https://CRAN.R-project.org/package=terra.

Ju, J., Masek, J.G., 2016. The vegetation greenness trend in Canada and US Alaska from 1984–2012 Landsat data. Remote Sens. Environ. 176, 1–16. https://doi.org/10.1016/j.rse.2016.01.001.

Kellndorfer, J.M., Walker, W.S., LaPoint, E., Kirsch, K., Bishop, J., Fiske, G., 2010. Statistical fusion of lidar, InSAR, and optical remote sensing data for forest stand height characterization: a regional-scale method based on LVIS, SRTM, Landsat ETM +, and ancillary data sets. *Journal of geophysical research*. Biogeosciences 115 (G2). https://doi.org/10.1029/2009JG000997.

Körner, C., Paulsen, J., 2004. A world-wide study of high altitude treeline temperatures. J. Biogeogr. 31 (5), 713–732. https://doi.org/10.1111/j.1365-2699.2003.01043.x.

Kurz, W.A., Shaw, C.H., Boisvenue, C., Stinson, G., Metsaranta, J., Leckie, D., Dyk, A., Smyth, C., Neilson, E.T., 2013. Carbon in Canada's boreal forest—a synthesis. Environ. Rev. 21 (4), 260–292. https://doi.org/10.1139/er-2013-0041.

Lang, N., Jetz, W., Schindler, K., Wegner, J.D., 2023. A high-resolution canopy height model of the earth. Nat. Ecol. Evol. 7 (11), Article 11. https://doi.org/10.1038/s41559-023-02206-6.

Lantz, T.C., Moffat, N.D., Fraser, R.H., Walker, X., 2019. Reproductive limitation mediates the response of white spruce (*Picea glauca*) to climate warming across the forest–tundra ecotone. Arctic Sci. 5 (4), 167–184. https://doi.org/10.1139/as-2018-0012.

Lefsky, M.A., 2010. A global forest canopy height map from the moderate resolution imaging Spectroradiometer and the geoscience laser altimeter system. Geophys. Res. Lett. 37 (15) https://doi.org/10.1029/2010GL043622.

Lefsky, M.A., Cohen, W.B., Harding, D.J., Parker, G.G., Acker, S.A., Gower, S.T., 2002. Lidar remote sensing of above-ground biomass in three biomes. Glob. Ecol. Biogeogr. 11 (5), 393–399. https://doi.org/10.1046/j.1466-822x.2002.00303.x.

Lim, K., Treitz, P., Wulder, M., St-Onge, B., Flood, M., 2003. LiDAR remote sensing of forest structure. Progr. Phys. Geogr.: Earth Environ.t 27 (1), 88–106. https://doi.org/10.1191/0309133303pp360ra.

Liu, A., Cheng, X., Chen, Z., 2021. Performance evaluation of GEDI and ICESat-2 laser altimeter data for terrain and canopy height retrievals. Remote Sens. Environ. 264, 112571 https://doi.org/10.1016/j.rse.2021.112571.

Loranty, M., Davydov, S., Kropp, H., Alexander, H., Mack, M., Natali, S., Zimov, N., 2018. Vegetation indices do not capture Forest cover variation in upland Siberian larch forests. Remote Sens. 10 (11), 1686. https://doi.org/10.3390/rs10111686.

Magruder, L., Brunt, K., Neumann, T., Klotz, B., Alonzo, M., 2021. Passive ground-based optical techniques for monitoring the on-orbit ICESat-2 altimeter geolocation and footprint diameter. Earth Space Sci. 8 (10) https://doi.org/10.1029/2020EA001414 e2020EA001414.

Maher, C.T., Dial, R.J., Pastick, N.J., Hewitt, R.E., Jorgenson, M.T., Sullivan, P.F., 2021. The climate envelope of Alaska's northern treelines: implications for controlling factors and future treeline advance. Ecography 44 (11), 1710–1722. https://doi.org/10.1111/ecog.05597.

Malambo, L., Popescu, S., Liu, M., 2023. Landsat-scale regional Forest canopy height mapping using ICESat-2 along-Track Heights: case study of eastern Texas. Remote Sens. 15 (1) https://doi.org/10.3390/rs15010001. Article 1.

Margolis, H.A., Nelson, R.F., Montesano, P.M., Beaudoin, A., Sun, G., Andersen, H.-E., Wulder, M.A., 2015. Combining satellite lidar, airborne lidar, and ground plots to estimate the amount and distribution of aboveground biomass in the boreal forest of North America. Can. J. For. Res. 45 (7), 838–855. https://doi.org/10.1139/cjfr-2015-0006.

Markus, T., Neumann, T., Martino, A., Abdalati, W., Brunt, K., Csatho, B., Farrell, S., Fricker, H., Gardner, A., Harding, D., Jasinski, M., Kwok, R., Magruder, L., Lubin, D., Luthcke, S., Morison, J., Nelson, R., Neuenschwander, A., Palm, S., Zwally, J., 2017. The ice, cloud, and land elevation Satellite-2 (ICESat-2): science requirements, concept, and implementation. Remote Sens. Environ. 190, 260–273. https://doi.org/10.1016/j.rse.2016.12.029.

Matasci, G., Hermosilla, T., Wulder, M.A., White, J.C., Coops, N.C., Hobart, G.W., Zald, H.S.J., 2018. Large-area mapping of Canadian boreal forest cover, height, biomass and other structural attributes using Landsat composites and lidar plots. Remote Sens. Environ. 209, 90–106. https://doi.org/10.1016/j.rse.2017.12.020.

Mengtian, H., Shilong, P., Zaichun, Z., Wang, T., Wu, D., Philippe, C., Myneni, R.B., Peaucelle, M., Shushi, P., Yang, H., Josep, P., 2017. Velocity of change in vegetation productivity over northern high latitudes. Nat. Ecol. Evol. 1 (11), 1649–1654. https://doi.org/10.1038/s41559-017-0328-y.

Montesano, P.M., Nelson, R., Sun, G., Margolis, H., Kerber, A., Ranson, K.J., 2009. MODIS tree cover validation for the circumpolar taiga–tundra transition zone. Remote Sens. Environ. 113 (10), 2130–2141. https://doi.org/10.1016/j.rse.2009.05.021.

Montesano, P.M., Sun, G., Dubayah, R.O., Ranson, K.J., 2016. Spaceborne potential for examining taiga-tundra ecotone form and vulnerability. Biogeosciences 13 (13), 3847–3861. https://doi.org/10.5194/bg-13-3847-2016.

Montesano, P.M., Neigh, C.S.R., Macander, M., Feng, M., Noojipady, P., 2020. The bioclimatic extent and pattern of the cold edge of the boreal forest: the circumpolar taiga-tundra ecotone. Environ. Res. Lett. 15 (10), 105019 https://doi.org/10.1088/1748-9326/abb2c7.

Mulverhill, C., Coops, N.C., Hermosilla, T., White, J.C., Wulder, M.A., 2022. Evaluating ICESat-2 for monitoring, modeling, and update of large area forest canopy height products. Remote Sens. Environ. 271, 112919 https://doi.org/10.1016/j.rse.2022.112919.

Myers-Smith, I.H., Hik, D.S., 2018. Climate warming as a driver of tundra shrubline advance. J. Ecol. 106 (2), 547–560. https://doi.org/10.1111/1365-2745.12817.

Myers-Smith, I.H., Forbes, B.C., Wilmking, M., Hallinger, M., Lantz, T., Blok, D., Tape, K.D., Macias-Fauria, M., Sass-Klaassen, U., Lévesque, E., Boudreau, S., Ropars, P., Hermanutz, L., Trant, A., Collier, L.S., Weijers, S., Rozema, J., Rayback, S.A., Schmidt, N.M., Hik, D.S., 2011. Shrub expansion in tundra ecosystems: dynamics, impacts and research priorities. Environ. Res. Lett. 6 (4), 045509 https://doi.org/10.1088/1748-9326/6/4/045509.

Narine, L.L., Popescu, S.C., Malambo, L., 2019. Synergy of ICESat-2 and Landsat for mapping Forest aboveground biomass with deep learning. Remote Sens. 11 (12) https://doi.org/10.3390/rs11121503. Article 12.

Nelson, R., 2010. Model effects on GLAS-based regional estimates of forest biomass and carbon. Int. J. Remote Sens. 31 (5), 1359–1372. https://doi.org/10.1080/01431160903380557.

Neuenschwander, A., Pitts, K., 2019. The ATL08 land and vegetation product for the ICESat-2 Mission. Remote Sens. Environ. 221, 247–259. https://doi.org/10.1016/j.rse.2018.11.005.

Neuenschwander, A., Guenther, E., White, J.C., Duncanson, L., Montesano, P., 2020. Validation of ICESat-2 terrain and canopy heights in boreal forests. Remote Sens. Environ. 251, 112110 https://doi.org/10.1016/j.rse.2020.112110.

Neuenschwander, A., Pitts, K.L., Jelley, B.P., Robbins, J., Klotz, B., Popescu, S.C., Nelson, R.F., Harding, D., Pederson, D., Sheridan, R., 2021. ATLAS/ICESat-2 L3A Land and Vegetation Height, Version 5 [dataset]. NASA National Snow and Ice Data Center DAAC. https://doi.org/10.5067/ATLAS/ATL08.005.

Neuenschwander, A., Magruder, L., Guenther, E., Hancock, S., Purslow, M., 2022. Radiometric assessment of ICESat-2 over vegetated surfaces. Remote Sens. 14 (3) https://doi.org/10.3390/rs14030787. Article 3.

Neumann, T.A., Martino, A.J., Markus, T., Bae, S., Bock, M.R., Brenner, A.C., Brunt, K.M., Cavanaugh, J., Fernandes, S.T., Hancock, D.W., Harbeck, K., Lee, J., Kurtz, N.T., Luers, P.J., Luthcke, S.B., Magruder, L., Pennington, T.A., Ramos-Izquierdo, L., Rebold, T., Thomas, T.C., 2019. The ice, cloud, and land elevation satellite – 2 mission: a global geolocated photon product derived from the advanced topographic laser altimeter system. Remote Sens. Environ. 233, 111325 https://doi.org/10.1016/j.rse.2019.111325.

Ni-Meister, W., Lee, S., Strahler, A.H., Woodcock, C.E., Schaaf, C., Yao, T., Ranson, K.J., Sun, G., Blair, J.B., 2010. Assessing general relationships between aboveground biomass and vegetation structure parameters for improved carbon estimate from lidar remote sensing. *Journal of geophysical research*. Biogeosciences 115 (G2). https://doi.org/10.1029/2009JG000936.

Olthof, I., Pouliot, D., 2010. Treeline vegetation composition and change in Canada's western subarctic from AVHRR and canopy reflectance modeling. Remote Sens. Environ. 114 (4), 805–815. https://doi.org/10.1016/j.rse.2009.11.017.

Olthof, I., Latifovic, R., Pouliot, D., 2009. Development of a circa 2000 land cover map of northern Canada at 30 m resolution from Landsat. Can. J. Remote. Sens. 15.

Orndahl, K.M., Macander, M.J., Berner, L.T., Goetz, S., 2022. Plant functional type aboveground biomass change within Alaska and Northwest Canada mapped using a 35-year satellite time series from 1985-2020. Environ. Res. Lett. https://doi.org/10.1088/1748-9326/ac9d50.

Payette, S., Fortin, M.-J., Gamache, I., 2001. The subarctic Forest–tundra: the structure of a biome in a changing climate: the shifting of local subarctic tree lines throughout the forest–tundra biome, which is linked to ecological processes at different spatiotemporal scales, will reflect future global changes in climate. BioScience 51 (9), 709–718. https://doi.org/10.1641/0006-3568(2001)051[0709:TSFTTS]2.0.CO;2.

Pearson, R.G., Phillips, S.J., Loranty, M.M., Beck, P.S.A., Damoulas, T., Knight, S.J., Goetz, S.J., 2013. Shifts in Arctic vegetation and associated feedbacks under climate change. Nat. Clim. Chang. 3 (7) https://doi.org/10.1038/nclimate1858. Article 7.

Queinnec, M., White, J.C., Coops, N.C., 2021. Comparing airborne and spaceborne photon-counting LiDAR canopy structural estimates across different boreal forest types. Remote Sens. Environ. 262, 112510 https://doi.org/10.1016/j.rse.2021.112510.

R Core Team, 2022. R: A Language and Environment for Statistical Computing. R Foundation for Statistical Computing. https://www.R-project.org/.

Ranson, K.J., Montesano, P.M., Nelson, R., 2011. Object-based mapping of the circumpolar taiga–tundra ecotone with MODIS tree cover. Remote Sens. Environ. 115 (12), 3670–3680. https://doi.org/10.1016/j.rse.2011.09.006.

Rees, W.G., Hofgaard, A., Boudreau, S., Cairns, D.M., Harper, K., Mamet, S., Mathisen, I., Swirad, Z., Tutubalina, O., 2020. Is subarctic forest advance able to keep pace with climate change? Glob. Chang. Biol. 26 (7), 3965–3977. https://doi.org/10.1111/gcb.15113.

Richardson, N., Cook, I., Crane, N., Dunnington, D., François, R., Keane, J., Moldovan-Grünfeld, D., Ooms, J., Arrow, Apache, 2022. arrow: Integration to "Apache "Arrow.". https://CRAN.R-project.org/package=arrow.

Schimel, D., Pavlick, R., Fisher, J.B., Asner, G.P., Saatchi, S., Townsend, P., Miller, C., Frankenberg, C., Hibbard, K., Cox, P., 2015. Observing terrestrial ecosystems and the carbon cycle from space. Glob. Chang. Biol. 21 (5), 1762–1776. https://doi.org/10.1111/gcb.12822.

Seider, J.H., Lantz, T.C., Hermosilla, T., Wulder, M.A., Wang, J.A., 2022. Biophysical determinants of shifting tundra vegetation productivity in the Beaufort Delta region of Canada. Ecosystems 25 (7), 1435–1454. https://doi.org/10.1007/s10021-021-00725-6.

Sexton, J.O., Song, X.-P., Feng, M., Noojipady, P., Anand, A., Huang, C., Kim, D.-H., Collins, K.M., Channan, S., DiMiceli, C., Townshend, J.R., 2013. Global, 30-m resolution continuous fields of tree cover: Landsat-based rescaling of MODIS vegetation continuous fields with lidar-based estimates of error. Intern. J. Digital Earth 6 (5), 427–448. https://doi.org/10.1080/17538947.2013.786146.

Shah, S.A.A., Manzoor, M.A., Bais, A., 2020. Canopy height estimation at Landsat resolution using convolutional neural networks. Mach. Learn. Knowled. Extract. 2 (1) https://doi.org/10.3390/make2010003. Article 1.

Simard, M., Pinto, N., Fisher, J.B., Baccini, A., 2011. Mapping forest canopy height globally with spaceborne lidar. J. Geophys. Res. Biogeosci. 116 (G4) https://doi.org/10.1029/2011JG001708.

Sothe, C., Gonsamo, A., Lourenço, R.B., Kurz, W.A., Snider, J., 2022. Spatially continuous mapping of Forest canopy height in Canada by combining GEDI and ICESat-2 with PALSAR and sentinel. Remote Sens. 14 (20) https://doi.org/10.3390/rs14205158. Article 20.

Sulla-Menashe, D., Woodcock, C.E., Friedl, M.A., 2018. Canadian boreal forest greening and browning trends: an analysis of biogeographic patterns and the relative roles of disturbance versus climate drivers. Environ. Res. Lett. 13 (1), 014007 https://doi.org/10.1088/1748-9326/aa9b88.

Sulphur, K.C., Goldsmith, S.A., Galloway, J.M., Macumber, A., Griffith, F., Swindles, G. T., Patterson, R.T., Falck, H., Clark, I.D., 2016. Holocene fire regimes and treeline migration rates in sub-arctic Canada. Glob. Planet. Chang. 145, 42–56. https://doi.org/10.1016/j.gloplacha.2016.08.003.

Tachikawa, T., Kaku, M., Iwasaki, A., Gesch, D., Oimoen, M., Danielson, J., Krieger, T., Curtis, B., Haase, J., Abrams, M., Carabajal, C., 2011. ASTER Global Digital Elevation Model Version 2—Summary of Validation Results. NASA.

Thieme, N., Martin Bollandsås, O., Gobakken, T., Næsset, E., 2011. Detection of small single trees in the forest–tundra ecotone using height values from airborne laser scanning. Can. J. Remote. Sens. 37 (3), 264–274. https://doi.org/10.5589/m11-041.

Timoney, K., 2022. Letter to the editor on "Satellite observations document trends consistent with a boreal biome shift.". Glob. Chang. Biol. 28 (18), 5335–5336. https://doi.org/10.1111/gcb.16327.

Timoney, K.P., Mamet, S., 2020. No treeline advance over the last 50 years in subarctic western and Central Canada and the problem of vegetation misclassification in remotely sensed data. Écoscience 27 (2), 93–106. https://doi.org/10.1080/11956860.2019.1698258.

Timoney, K.P., La Roi, G.H., Zoltai, S.C., Robinson, A.L., 1992. The high subarctic Forest-tundra of northwestern Canada: position, width, and vegetation gradients in relation to climate. ARCTIC 45 (1), 1–9. https://doi.org/10.14430/arctic1367.

Travers-Smith, H.Z., Lantz, T.C., 2020. Leading-edge disequilibrium in alder and spruce populations across the forest–tundra ecotone. Ecosphere 11 (7), e03118. https://doi.org/10.1002/ecs2.3118.

Vincent, L.A., Hartwell, M.M., Wang, X.L., 2020. A third generation of homogenized temperature for trend analysis and monitoring changes in Canada's climate. Atmosphere-Ocean 58 (3), 173–191. https://doi.org/10.1080/07055900.2020.1765728.

Virkkala, A.-M., Aalto, J., Rogers, B.M., Tagesson, T., Treat, C.C., Natali, S.M., Watts, J. D., Potter, S., Lehtonen, A., Mauritz, M., Schuur, E.A.G., Kochendorfer, J., Zona, D., Oechel, W., Kobayashi, H., Humphreys, E., Goeckede, M., Iwata, H., Lafleur, P.M., Luoto, M., 2021. Statistical upscaling of ecosystem CO2 fluxes across the terrestrial tundra and boreal domain: regional patterns and uncertainties. Glob. Chang. Biol. 27 (17), 4040–4059. https://doi.org/10.1111/gcb.15659.

Walker, X.J., Alexander, H.D., Berner, L.T., Boyd, M.A., Loranty, M.M., Natali, S.M., Mack, M.C., 2021. Positive response of tree productivity to warming is reversed by increased tree density at the Arctic tundra–taiga ecotone. Can. J. For. Res. 51 (9), 1323–1338. https://doi.org/10.1139/cjfr-2020-0466.

Wang, J.A., Friedl, M.A., 2019. The role of land cover change in Arctic-boreal greening and browning trends. Environ. Res. Lett. 14 (12), 125007 https://doi.org/10.1088/1748-9326/ab5429.

Wang, J.A., Sulla-Menashe, D., Woodcock, C.E., Sonnentag, O., Keeling, R.F., Friedl, M. A., 2020. Extensive land cover change across Arctic–Boreal Northwestern North America from disturbance and climate forcing. Glob. Chang. Biol. 26 (2), 807–822. https://doi.org/10.1111/gcb.14804.

Wang, T., Hamann, A., Spittlehouse, D., Carroll, C., 2016. Locally downscaled and spatially customizable climate data for historical and future periods for North America. PLoS One 11 (6), e0156720. https://doi.org/10.1371/journal.pone.0156720.

White, J.C., Wulder, M.A., Hobart, G.W., Luther, J.E., Hermosilla, T., Griffiths, P., Coops, N.C., Hall, R.J., Hostert, P., Dyk, A., Guindon, L., 2014. Pixel-based image compositing for large-area dense time series applications and science. Can. J. Remote. Sens. 40 (3), 192–212. https://doi.org/10.1080/07038992.2014.945827.

Wickham, H., 2016. ggplot2: Elegant Graphics for Data Analysis. Springer-Verlag, New York. https://ggplot2.tidyverse.org.

Wickham, H., François, R., Henry, L., Müller, K., 2022. dplyr: A Grammar of Data Manipulation. https://CRAN.R-project.org/package=dplyr.

Wilmking, M., Harden, J., Tape, K., 2006. Effect of tree line advance on carbon storage in NW Alaska. J. Geophys. Res. Biogeosci. 111 (G2) https://doi.org/10.1029/2005JG000074.

Wright, M.N., Ziegler, A., 2017. Ranger: a fast implementation of random forests for high dimensional data in C++ and R. J. Stat. Softw. 77 (1), 1–17. https://doi.org/10.18637/jss.v077.i01.

Wulder, M.A., White, J.C., Bater, C.W., Coops, N.C., Hopkinson, C., Chen, G., 2012. Lidar plots — a new large-area data collection option: context, concepts, and case study. Can. J. Remote. Sens. 38 (5), 600–618. https://doi.org/10.5589/m12-049.

Zhang, T., Liu, D., 2023. Improving ICESat-2-based boreal forest height estimation by a multivariate sample quality control approach. Methods Ecol. Evol. 14 (7), 1623–1638. https://doi.org/10.1111/2041-210X.14112.